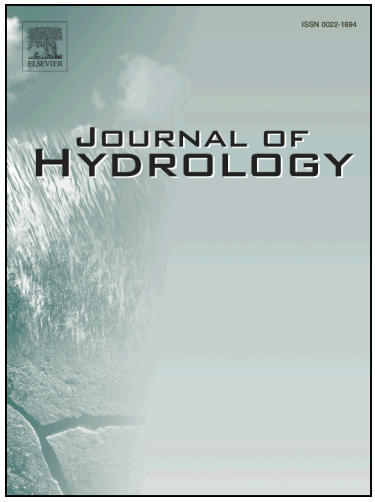

Research papers

Monitoring snow cover variability (2000–2014) in the Hengduan Mountains based on cloud-removed MODIS products with an adaptive spatio-temporal weighted method

Xinghua Li, Wenxuan Fu, Huanfeng Shen, Chunlin Huang, Liangpei Zhang

PII: S0022-1694(17)30342-6
DOI: http://dx.doi.org/10.1016/j.jhydrol.2017.05.049
Reference: HYDROL 22040

To appear in: *Journal of Hydrology*

Received Date: 29 April 2016
Revised Date: 23 May 2017
Accepted Date: 24 May 2017

Please cite this article as: Li, X., Fu, W., Shen, H., Huang, C., Zhang, L., Monitoring snow cover variability (2000–2014) in the Hengduan Mountains based on cloud-removed MODIS products with an adaptive spatio-temporal weighted method, *Journal of Hydrology* (2017), doi: http://dx.doi.org/10.1016/j.jhydrol.2017.05.049

Monitoring snow cover variability (2000–2014) in the Hengduan Mountains based on cloud-removed MODIS products with an adaptive spatio-temporal weighted method

Xinghua Li [a], Wenxuan Fu [b], Huanfeng Shen [c,d,e,*], Chunlin Huang [f], Liangpei Zhang [e,g]

[a] *School of Remote Sensing and Information Engineering, Wuhan University, Wuhan 430079, China*

[b] *Sanya Surveying and Mapping Technology Center of Development and Service, NASG, Sanya 572029, China*

[c] *School of Resource and Environmental Sciences, Wuhan University, Wuhan 430079, China*

[d] *Key Laboratory of Geographic Information System, Ministry of Education, Wuhan University, Wuhan 430079, China*

[e] *Collaborative Innovation Center for Geospatial Information Technology, Wuhan University, Wuhan 430079, China*

[f] *Key Laboratory of Remote Sensing of Gansu Province, Heihe Remote Sensing Experimental Research Station, Northwest Institute of Eco-Environment and Resources, Chinese Academy of Sciences, Lanzhou 730000, China*

[g] *State Key Laboratory of Information Engineering in Surveying, Mapping, and Remote Sensing, Wuhan University, Wuhan 430079, China*

* Corresponding author.

E-mail address: shenhf@whu.edu.cn.

Abstract:

Monitoring the variability of snow cover is necessary and meaningful because snow cover is closely connected with climate and ecological change. In this work, 500m resolution MODIS daily snow cover products from 2000 to 2014 were adopted to analyze the status in Hengduan Mountains. In order to solve the spatial discontinuity caused by clouds in the products, we propose an adaptive spatio-temporal weighted method (ASTWM), which is based on the initial result of a Terra and Aqua combination. This novel method simultaneously considers

the temporal and spatial correlations of the snow cover. The simulated experiments indicate that ASTWM removes clouds completely, with a robust overall accuracy (OA) of above 93% under different cloud fractions. The spatio-temporal variability of snow cover in the Hengduan Mountains was investigated with two indices: snow cover days (SCD) and snow fraction. The results reveal that the annual SCD gradually increases and the coefficient of variation (CV) decreases with elevation. The pixel-wise trends of SCD first rise and then drop in most areas. Moreover, intense intra-annual variability of the snow fraction occurs from October to March, during which time there is abundant snow cover. The inter-annual variability, which mainly occurs in high elevation areas, shows an increasing trend before 2004/2005 and a decreasing trend after 2004/2005. In addition, the snow fraction responds to the two climate factors of air temperature and precipitation. For the intra-annual variability, when the air temperature and precipitation decrease, the snow cover increases. Besides, precipitation plays a more important role in the inter-annual variability of snow cover than temperature.

Keywords:

Cloud-removal method; Hengduan Mountains; MODIS; Snow cover; Spatio-temporal weighted method

1. Introduction

Snow is a significant element of the cryosphere, affecting the energy balance, climate, ecology, and hydrology, and even the activities of human beings (Barnett et al., 1988; Robinson et al., 1993; Brown, 2000). In the Hengduan Mountains, snowmelt water is an essential water resource, contributing a lot to the runoff and supporting lives downstream (Flerchinger et al., 1992; Singh et al., 2006). Moreover, snow cover is sensitive to regional climate change, which perhaps differs from global climate change (Barnett et al., 1989; Barnett et al., 2005; Dahe et al., 2006). In addition, as a global biodiversity hotspot, the Hengduan Mountains provide a stable beneath-the-snow refuge for plants and animals, which gives essential relief from biting winds

and subzero temperatures in harsh winter weather (Pauli et al., 2013). However, with the rapid growth of human activities, the ecological balance is broken and climate is changed, which results in a decline in natural resources and an acceleration of species extinction. Consequently, it is necessary and meaningful to monitor the spatial and temporal variability of snow cover in the Hengduan Mountains.

Because of the high spatial and temporal resolution, MODIS snow cover products are widely used in the monitoring of snow cover (Hall et al., 2002). Many studies have proved that the products show a relatively high agreement with the *in situ* observations or other remote sensing images under clear-sky conditions in different scales (Bitner et al., 2002; Klein and Barnett, 2003; Simic et al., 2004; Déry et al., 2005; Parajka and Blöschl, 2006; Tong et al., 2009a; Parajka and Blöschl, 2012). However, the clouds in these products are so severe that their application is limited, which is a very common phenomenon in remote sensing data (Parajka and Blöschl, 2006; Cheng et al., 2014; Li et al., 2014). Therefore, a number of methods have been proposed to remove clouds from MODIS snow cover products, but these cloud-removal methods differ from the regular cloud-removal methods of remote sensing data (Cheng et al.; Zeng et al., 2013; Li et al., 2015; Shen et al., 2015; Li et al., 2016). The MODIS cloud-removal methods can be classified into three main categories: spatial methods, temporal methods, and spatio-temporal hybrid methods.

For the spatial methods, the simplest spatial filter is based on the cloud-free observations in the four or eight neighboring pixels (Parajka and Blöschl, 2008; Gafurov and Bárdossy, 2009; Tong et al., 2009a; Paudel and Andersen, 2011; López-Burgos et al., 2013). With this method, clouds with a fraction of less than 10% can be removed. With the introduction of an auxiliary DEM, the snow transition elevation method and the regional snowline mapping method assign cloud pixels based on the snowline and the landline, respectively. All the cloud pixels above the snowline are considered to be snow, and all the cloud pixels below the landline are considered to be “no snow” (Gafurov and Bárdossy, 2009; Parajka et al., 2010). These methods perform well in both high and low elevations. However, the greater the cloud fraction, the lower the

accuracy. Paudel and Andersen (2011) and Da Ronco and De Michele (2014) took into consideration topography and land use to improve this approach. The locally weighted logistic regression method estimates the snow occurrence probability of a cloud pixel by its topographic relationship with the surrounding cloud-free pixels (López-Burgos et al., 2013). This method obtains a satisfactory accuracy, but comes with a high computational cost. The above methods mainly make use of the spatial correlations; however, when the cloud fraction is high, it is difficult to guarantee their accuracy.

The temporal methods are based on the time-series correlations of snow cover. The most widely used temporal method is the Terra and Aqua combination, which can remove between 5–20% of the cloud cover (Parajka and Blöschl, 2008; Gafurov and Bárdossy, 2009; Wang et al., 2009; Xie et al., 2009; Gao et al., 2010; Paudel and Andersen, 2011; Da Ronco and De Michele, 2014) with a slightly lower accuracy than the original products. This approach benefits from the fact that cloud distribution is changeable within an interval of three hours. Adjacent temporal deduction is another useful method, exploiting the information in predefined preceding and following temporal windows (Gafurov and Bárdossy, 2009; Gao et al., 2010; Paudel and Andersen, 2011; López-Burgos et al., 2013; Da Ronco and De Michele, 2014). This approach is based on the assumption that snow remains constant in the temporal windows, so the accuracy in a "snow-stable" period is higher than that in a "snow-transitional" period. In addition, both the temporal filter and multi-temporal combination only use the snow cover information of the preceding days to remove clouds. The temporal filter, which replaces cloud pixels by the most recent preceding cloud-free observations (Parajka and Blöschl, 2008; Hall et al., 2010; Parajka et al., 2012; Da Ronco and De Michele, 2014), can keep the temporal resolution of snow cover products. The multi-temporal combination replaces the cloud pixels by the cloud-free observations in a fixed or flexible temporal window from between 1 to 8 days while decreasing the temporal resolution (Şorman et al., 2007; Liang et al., 2008; Wang et al., 2009; Gao et al., 2010). However, the two methods cannot remove the clouds completely and may lose the information about short snowfall events. In contrast, the seasonal filter uses a

longer time series to remove the remaining clouds completely. It assumes that a hydrologic year has only one snow cycle, and sets two thresholds for each pixel, i.e., the snow melt day and snow accumulation day (Gafurov and Bárdossy, 2009). Nevertheless, it ignores the multiple snow cycles in a hydrologic year for some regions. Thus, Paudel and Andersen (2011) introduced the thresholds of the snow accumulation day, the minimum snow extent day, and the maximum snow extent day in each snow cycle. This approach works well when a hydrologic year has several snow cycles. In general, these temporal methods can obtain a good cloud removal accuracy by the use of simple ideas, but they fail in the condition of cloud cover persisting for a long time in the same area.

Most of the spatial or temporal methods cannot remove clouds completely, despite the high cloud removal accuracy. Moreover, it is known that the spatial and temporal methods have some advantages which can complement each other. Hence, the two kinds of methods can be combined step by step for a better removal effect (Gafurov and Bárdossy, 2009; Paudel and Andersen, 2011; López-Burgos et al., 2013; Da Ronco and De Michele, 2014). The sequential combination methods remove clouds completely and can acquire a better accuracy than the spatial or temporal methods. However, they independently utilize the spatial or temporal characteristics of the snow cover in the corresponding step, and they cannot make full use of the spatial and temporal correlations of snow cover. To this end, an innovative joint spatio-temporal method named the adaptive spatio-temporal weighted method (ASTWM) is proposed in this paper. The basic idea of ASTWM is that topography has a prominent influence on the spatial distribution of snow cover, while the characteristics of snow cover remain relatively similar in a short time series. This approach has the great advantage of considering the spatial and temporal correlations of the snow cover simultaneously. Furthermore, it can be adopted as a separate cloud removal method or as the last step when combined with other methods.

On the other hand, the hydrological applications of MODIS snow cover products mainly concentrate on the analysis of the variability of snow cover, snowmelt runoff simulation, input

parameters of the hydrological and meteorological model, and the aided generation of snow water equivalent or snow depth product, and so on. Maskey et al. (2011) made an analysis of snow cover changes in the Himalayan region (2000–2008) using MODIS 8-day composite snow products and *in situ* temperature data, which demonstrates the snow cover has a strong negative correlation with the temperature. Paudel and Andersen (2011) researched the snow cover variability in the Trans Himalayan region of Nepal using MODIS data with improved cloud removal methodology, and the peak snow period has been delayed by about 6.7 days per year from 2000 to 2010. Wang and Xie (2009) monitored the spatio-temporal variation of snow cover in northern Xinjiang, China, with the snow cover index (SCI), snow cover day/duration (SCD), snow cover onset dates (SCOD) and snow cover melting dates (SCMD). Further, Wang et al (2015) also monitored Tibetan Plateau, and discovered the maximum number of SCD in a year followed a decreasing tendency from 2003 to 2010. Tong et al. (2009b) investigated the relationship between snow cover and terrain in an alpine watershed of western Canada, and it indicates the snow cover duration is positively correlated to the elevation. In addition, there is no evidence of a statistically significant long-term trend over the Moroccan Atlas mountain range (Marchane et al., 2015). Snow cover duration anomalies reveal a deficient snowpack on the Spanish side of the Pyrenees, which seems to have caused a drop in the national hydropower production (Gascoin et al., 2015). The previous research has exposed that snow cover can quantify the possible effects of abnormal weather conditions and predict future scenarios (Dietz et al., 2012).

On the whole, this paper aims to achieve two goals. The first is to propose the ASTWM cloud removal method, which is more suitable for mountainous regions. For a higher OA, ASTWM is combined with the Terra and Aqua combination. Then, based on the result of the proposed method, the second goal is to detect the spatial and temporal variability of snow cover in response to climate change from 2000 to 2014 in the Hengduan Mountains.

The rest of this paper is organized as follows. In Section 2, the study area and the data, which include remote sensing data, digital elevation data, and meteorological data, are introduced. The cloud removal methods of the Terra and Aqua combination and ASTWM are described in Section 3. The cloud removal accuracy of the proposed method is evaluated and the variability of snow cover in the Hengduan Mountains is analyzed in Section 4. Finally, the discussion and conclusion are provided in Section 5.

2. Study area and data

2.1. Study area

The study area is the Hengduan Mountains, located between 25°W to 33°W and 96°E to 104°E, with a total area of approximately 35000km^2 (Fig. 1). The name *Hengduan* means "to transect", and this range is one of China's few north–south ranges, cutting perpendicular to the Himalayas. The northern part of the Hengduan Mountains lies to the west of the Sichuan Basin and includes the Min and Qionglai mountain ranges. The southern part borders complex river gorge country where rivers from southeastern Tibet spill into Southeast Asia. The area includes a complex of ridges and river valleys, with the maximum altitude falling gradually from over 7000m in the north to 500–2000m in the south. The elevation of most of the ridges is between 4000m to 5000m. The Gongga Mountain, located about 30°W, reaches 7556m above sea level, and is the culmination of the study area. The Yulong Mountain, located about 27°W, reaches 5596 m above sea level, and is the area of glaciers in the most southern latitude of China. With regard to climate, with the influence of the upper west wind, the Indian Ocean, and the Pacific monsoon circulation, the area is arid in winter and wet in summer. In general, during the monsoon from mid-May to mid-October, most of the precipitation occurs, accounting for more than 85% of the yearly total. In fact, the precipitation occurs mainly in June, July, and August. The subtropical latitude and the monsoonal climate, together with the great altitudinal range, have produced a natural flora and fauna that ranks among the richest and most varied in the world.

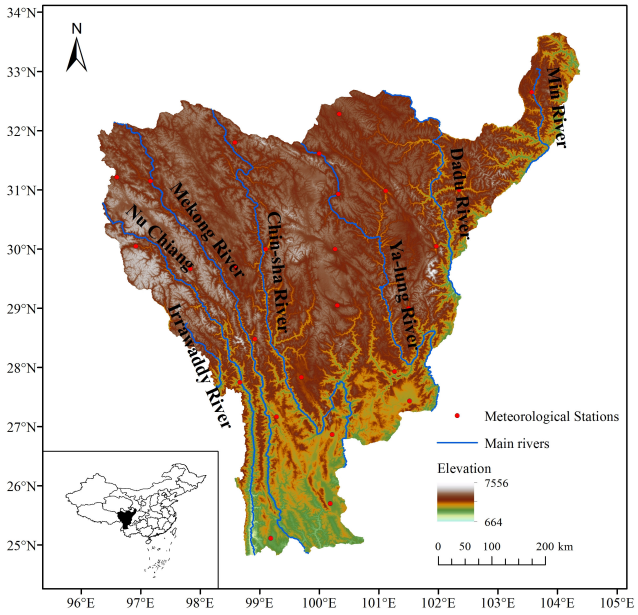

Fig. 1. The location and elevation distribution of Hengduan Mountains.

2.2. Data

The snow cover data in MODIS Terra/Aqua Snow Cover Daily L3 Global 500m Grid Version 5 (MOD10A1/MYD10A1) (Hall et al., 2007) were used in this study. The snow cover data comprise 11 classes in total, including snow, lake ice, no snow/land, lake, ocean, sensor data missing, no decision, night, detector saturated, and fill, based on a snow mapping algorithm that employs the normalized difference snow index (NDSI) and other criteria tests (Hall et al., 2001; Hall et al., 2002; Riggs et al., 2006; Salomonson and Appel, 2006). All the MODIS snow cover products from September 1, 2000, to August 31, 2014, were obtained from the National Snow and Ice Data Center (NSIDC, http://nsidc.org), with tiles H26V05, H26V06, and H27V06 covering the whole study area. Because MYD10A1 is only available from July 4, 2002, MOD10A1 were utilized from that time. The MODIS Reprojection Tool (MRT) was used to mosaic the three tiles and reproject them into Universal Transverse Mercator (UTM) coordinates. After the pre-processing, the original snow cover data were reclassified into three categories. Specifically, the snow and lake ice classes were reclassified into the snow category; the no snow (land), lake, and ocean classes were reclassified into the no snow category; and the

cloud and other classes were reclassified into the cloud category. The coded integer values for the three categories were 200, 50, and 1, respectively.

The ancillary data were the NASA Shuttle Radar Topographic Mission (SRTM) 90m digital elevation data, which were obtained from the CGIAR Consortium for Spatial Information (CGIAR–CSI, http://srtm.csi.cgiar.org). Aiming to match the MODIS snow cover products, the DEM data were resampled into a 500m spatial resolution and reprojected into UTM coordinates.

In addition, monthly average air temperature and monthly precipitation data were downloaded from 26 meteorological stations of the China Meteorological Data Sharing Service System (see Fig. 1, http://cdc.nmic.cn). The air temperature and precipitation data for the period of September 2000 to August 2014 were used to analyze the relationship with the snow fraction.

3. Methodology

A two-step method is proposed to remove clouds completely from the MODIS snow cover products. The output of the first step, the Terra and Aqua combination, is the input of the second step, ASTWM. The schematic diagram is shown in Fig. 2.

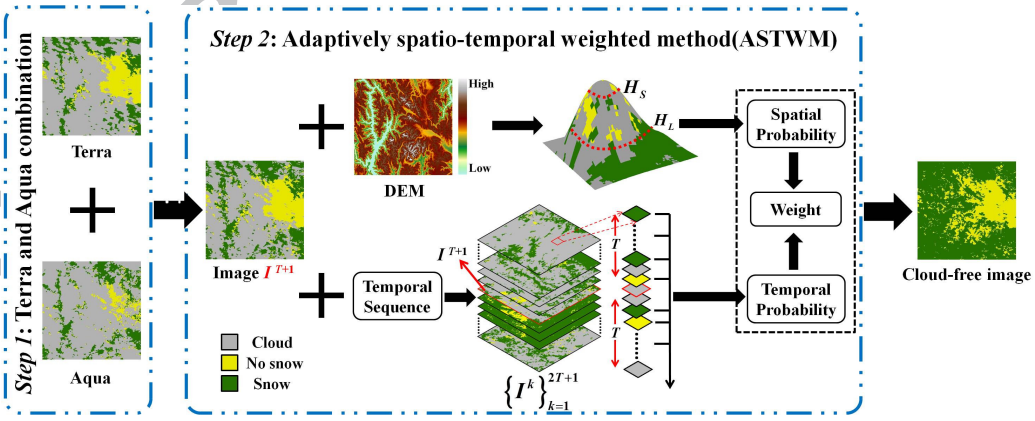

Fig. 2. Schematic diagram of the two-step cloud removal method.

3.1. Terra and Aqua combination

The first step combines the Terra and Aqua snow cover products on the same day into one product with less clouds, based on the fact that the Terra and Aqua satellites observe the same area of the Earth approximately three hours apart, during which time the clouds can move. The combination rule is: 1) if a pixel is observed as snow by either satellite, the pixel is assigned as snow ; 2) if a pixel is observed as no snow by one satellite and cloud by another, the pixel is assigned as no snow; 3) if a pixel is observed as cloud by both satellites, the pixel is assigned as cloud; and 4) if only the Terra (or Aqua) snow cover product is available on a certain day, it is regarded as the output of this step. In other words, if a pixel in one of the product (Terra or Aqua) is classified as snow and the pixel in other product is classified as land, it will be considered as snow.

3.2. The adaptive spatio-temporal weighted method (ASTWM)

Many studies have demonstrated that snow fraction exhibits a positive linear correlation with elevation (Tong et al., 2009b; Sharma et al., 2014; Jin et al., 2015). Moreover, the closer the time interval, the more similar are the characteristics of snow. The present methods just make a sequential combination of the spatial and temporal correlations of the snow cover, which does not make full use of the available information. Thus, we propose ASTWM, which simultaneously takes advantage of the spatial and temporal correlations of the snow cover. In the proposed approach, the cloud removal is realized by estimating the probability of the snow cover. When the probability is equal to or greater than a threshold, a cloud pixel is assigned as snow; otherwise, it is assigned as no snow. Specifically, the probability is the weighted combination of the spatial probability and temporal probability, which are estimated by the snow cover information in the spatial and temporal dimensions, respectively.

The snow cover product used in the cloud removal is defined as I^{T+1}, on the assumption that there is a temporal sequence of products $\left\{I^k\right\}_{k=1}^{2T+1}$, where T is the number of the preceding and following days for I^{T+1}. Hence, the snow probability of a cloud pixel can be expressed by Eq. (1):

$$P_{(i,j)}^{S} = w_{(i,j)} \times P_{(i,j)}^{H} + \left(1 - w_{(i,j)}\right) \times P_{(i,j)}^{T} \quad (1)$$

where i and j are the indices of the rows and columns in $\left\{I^{k}\right\}_{k=1}^{2T+1}$; $P_{(i,j)}^{S}$ is the resulting probability of snow for the cloud pixel; $P_{(i,j)}^{H}$ and $P_{(i,j)}^{T}$ are the spatial and temporal probabilities of snow for the cloud pixel, respectively; and $w_{(i,j)}$ is the weight of $P_{(i,j)}^{H}$.

Since the binary snow cover data only include snow and no snow pixels, to classify the cloud pixels into snow or no snow is an equal possibility event. Therefore, the threshold of $P_{(i,j)}^{S}$ is set to 0.5. When $P_{(i,j)}^{S}$ is equal to or greater than 0.5, the cloud pixel is assigned as snow; otherwise, the cloud pixel is assigned as no snow. In the following, $P_{(i,j)}^{H}$, $P_{(i,j)}^{T}$, and $w_{(i,j)}$ are described in detail.

3.2.1. The spatial probability of snow

$P_{(i,j)}^{H}$ is actually estimated by the relationship between the elevation and the snow fraction. First of all, the snowline, which is similar to the regional snowline of (Parajka et al., 2010), is utilized. The snowline H_S is the elevation above which all the cloud-free pixels are observed as snow. Similarly, the landline H_L is the elevation below which all the cloud-free pixels are observed as no snow. The elevation between H_S and H_L is then divided into several elevation zones with a 100-m interval. At the same time, the elevations above H_S and below H_L are also regarded as single elevation zones, respectively. Accordingly, in any elevation zone, the spatial probability of snow is estimated by the ratio of the number of snow pixels N_H^s to the number of cloud-free pixels N_H^{nc}. However, due to the heavy cloud and complex land-cover types, the snow fraction does not always exhibit a linear correlation with elevation. Therefore, a constraint is added to $P_{(i,j)}^{H}$ to reduce its contribution to the resulting probability of snow. The improved spatial probability of snow $P_{(i,j)}^{H}$ can be expressed by Eq. (2):

$$P_{(i,j)}^{H} = \frac{N_H^s \times (1-\xi)}{N_H^{nc}} \tag{2}$$

where ξ is the cloud fraction in the snow cover product I^{T+1}. It is noteworthy that if there are no cloud-free pixels in an elevation zone, only $P_{(i,j)}^{T}$ is used to reclassify the cloud pixels.

3.2.2. The temporal probability of snow

$P_{(i,j)}^{T}$ is estimated by the information in the cloud-free observations in the preceding and following days. In the time series, every observation provides a component of the temporal probability of the cloud pixel, and their weighted sum is the final temporal probability. As we know, snow characteristics are closely related to time, and a shorter interval usually means a closer relationship. Thus, the time interval $d_{(i,j)}$ between the cloud-free day and the current day is regarded as the weight to acquire the temporal probability of snow. According to the characteristics of the temporal correlation, the weight is calculated in a similar way to the inverse distance weighted method. As a result, $P_{(i,j)}^{T}$ can be expressed by Eq. (3):

$$P_{(i,j)}^{T} = \frac{\sum_{k=1}^{2T+1} \left[p_{(i,j)}^{k} / d_{(i,j)}^{k} \right]}{\sum_{k=1}^{2T+1} \left(1 / d_{(i,j)}^{k} \right)} \left(I_{(i,j)}^{k} \neq 1 \right) \tag{3}$$

where

$$p_{(i,j)}^{k} = \begin{cases} 1, & \text{if } I_{(i,j)}^{k} = 200 \\ 0, & \text{if } I_{(i,j)}^{k} = 50 \end{cases} \tag{4}$$

For the Hengduan Mountains, $T = 15$ was chosen to remove clouds for the reason that 15 days could guarantee sufficient cloud-free observations.

3.2.3. The weighting

As stated above, if a cloud pixel is assigned as snow, $P_{(i,j)}^{S}$ should be no less than 0.5, namely:

$$\left(P_{(i,j)}^{H} - P_{(i,j)}^{T} \right) \times w_{(i,j)} + P_{(i,j)}^{T} \geq 0.5 \tag{5}$$

For Eq. (5), three situations occur:

(a) if $P_{(i,j)}^{H} > P_{(i,j)}^{T}$, $w_{(i,j)} \geq \frac{0.5 - P_{(i,j)}^{T}}{P_{(i,j)}^{H} - P_{(i,j)}^{T}}$;

(b) if $P_{(i,j)}^{H} = P_{(i,j)}^{T}$, $w_{(i,j)}$ does not make a contribution to Eq. (5);

(c) if $P_{(i,j)}^{H} < P_{(i,j)}^{T}$, $w_{(i,j)} \leq \frac{0.5 - P_{(i,j)}^{T}}{P_{(i,j)}^{H} - P_{(i,j)}^{T}}$.

$w_{(i,j)}$ is estimated by the cloud-free pixels of I^{T+1}. For different snow cover products, the distributions of cloud and snow cover vary, so that $w_{(i,j)}$ should also be different. In order to weight the spatial and temporal probability of snow automatically, a sensitivity analysis is applied to calculate $w_{(i,j)}$ under situations (a) and (c), respectively. It is assumed that cloud pixels of I^{T+1} have the same $w_{(i,j)}$ as the cloud-free pixels, defined as w_H. Firstly, in the same way we acquire $P_{(i,j)}^{S}$, the resulting snow probability of the cloud-free pixel ($\overline{P_{(i,j)}^{S}}$) is acquired by Eq. (1). Secondly, we change the value of w_H to maximize the OA of the cloud-free pixels, i.e., w_H is varied from 0 to 1 with a step size of 0.01. The corresponding w_H is regarded as the weight $w_{(i,j)}$ of $P_{(i,j)}^{S}$. In other words, the weight $w_{(i,j)}$ is calculated by the cloud-free pixels.

3.3. The validation methods

3.3.1. The cloud removal accuracy of snow cover

The *in situ* observation datasets are sparsely distributed in the elevation from 1500 m to 4000 m in the study area, as shown in Fig. 1. In addition, it is not reasonable to use an *in situ* observation to represent a pixel value of a product with an area of about 0.25 km^2. For the above reasons, the validation method proposed by Gafurov and Bárdossy (2009) was adopted in the simulated experiments. Firstly, the original cloud-less Terra snow cover product (with a cloud fraction of less than 5%) was considered as the "truth". The cloud masks (with different fractions) from the other products were then used to cover the "truth" and produce the new

products as “observations”. Finally, the cloud removal results of the “observations” were compared with the “truth” by the OA, the overall clear-sky accuracy (OC), the underestimation error (UE), and the overestimation error (OE), which are expressed as follows:

$$\mathrm{OA} = \frac{N_s^s + N_{ns}^{ns}}{N_a} \tag{6}$$

$$\mathrm{OC} = \frac{N_s^s + N_{ns}^{ns}}{N_c} \tag{7}$$

$$\mathrm{OE} = \frac{N_s^{ns}}{N_c} \tag{8}$$

$$\mathrm{UE} = \frac{N_{ns}^s}{N_c} \tag{9}$$

where N_s^s is the total number of cloud pixels which are assigned as snow in the “observations” and are observed as snow in the “truth”; N_{ns}^{ns} is the total number of cloud pixels which are assigned as no snow in the “observations” and are observed as no snow in the “truth”; N_s^{ns} is the total number of cloud pixels which are assigned as snow in the “observations” and are observed as no snow in the “truth”; N_{ns}^s is the total number of cloud pixels which are assigned as no snow in the “observations” and are observed as snow in the “truth”; N_a is the total number of cloud pixels in the “observations”; and N_c is the total number of cloud pixels which are assigned in the “observations”.

3.3.2. The variability of snow cover

The snow cover variability is analyzed by the use of the snow cover days (SCD) and snow fraction. SCD is the total number of days with snow cover in a hydrologic year (Wang and Xie, 2009; Tang et al., 2013), and snow fraction is the percentage of snow pixels in a given area. In this study, September 1 to the following August 31 is regarded as a hydrologic year. The SCD is calculated by individual pixels and is expressed as shown in Eq. (10):

$$\mathrm{SCD}_{(i,j)} = \sum_{k=1}^{n} p_{(i,j)}^k \tag{10}$$

where n is the sum of days in a hydrologic year, and $p_{(i,j)}^k$ is defined as shown in Eq. (4).

For SCD, we show the distribution of the average SCD from 2000 to 2014 with the

coefficient of variation (CV), followed by the pixel-wise trends obtained by the use of a piecewise linear regression model with one breakpoint (Toms and Lesperance, 2003; Wang et al., 2011):

$$y = \begin{cases} \beta_0 + \beta_1 t + \varepsilon, & t \le \alpha \\ \beta_0 + \beta_1 t + \beta_2 (t - \alpha) + \varepsilon, & t > \alpha \end{cases} \quad (11)$$

where y is the SCD or snow fraction; t is the year; α is the breakpoint of the trend, as determined by the least square error method; β_0, β_1, and β_2 are the regression coefficients; and ε is the residual error. β_1 and $\beta_1 + \beta_2$ are the trends before and after the breakpoint, respectively.

For the snow fraction, both the intra-annual variability and the inter-annual variability are monitored. The intra-annual variability is based on the average daily snow fraction. The inter-annual variability is based on the average annual snow fraction in the whole region and under the different elevation zones. The piecewise linear regression model was again applied to study the trends.

4. Results and analysis

4.1. Evaluation of the cloud removal methods

A number of verification experiments were conducted. Firstly, the effectiveness of the proposed method was evaluated with regard to the cloud fraction. In terms of the proposed method, the first step is the Terra and Aqua combination, and the second step is ASTWM. This method was compared with the temporal filter (Parajka and Blöschl, 2008), which was also applied after the Terra and Aqua combination. Secondly, the accuracy of the cloud removal was further assessed by simulated experiments, in which only ASTWM and the temporal method (Parajka and Blöschl, 2008) were used for the cloud removal, with the first step omitted. The comparison method also includes the combination of temporal filter and spatial filter (Parajka and Blöschl, 2008).

4.1.1. Effectiveness of the cloud removal methods

Fig. 3 shows the real average monthly cloud fraction of Terra, Aqua, and the remaining fraction after each step, including the Terra and Aqua combination, the temporal filter, and the proposed ASTWM. For the original snow cover products, the intra-annual cloud fraction in the Hengduan Mountains is high in summer and low in winter. Furthermore, the cloud fraction of the Aqua products is higher than the Terra products. After the Terra and Aqua combination, the cloud fraction is reduced by 7–13% compared to the Terra product. However, the cloud fraction is higher than 20% in most months. Based on the result of the first step, the temporal filter clearly reduces the cloud fraction, but not completely. It remains at 1% in winter and almost 20% in summer, which does influence the analysis of the snow cover variability to some degree. In contrast, ASTWM removes all the clouds successfully, and it is the only method that achieves this goal. This experiment demonstrates that ASTWM is the most effective method and can remove the clouds completely.

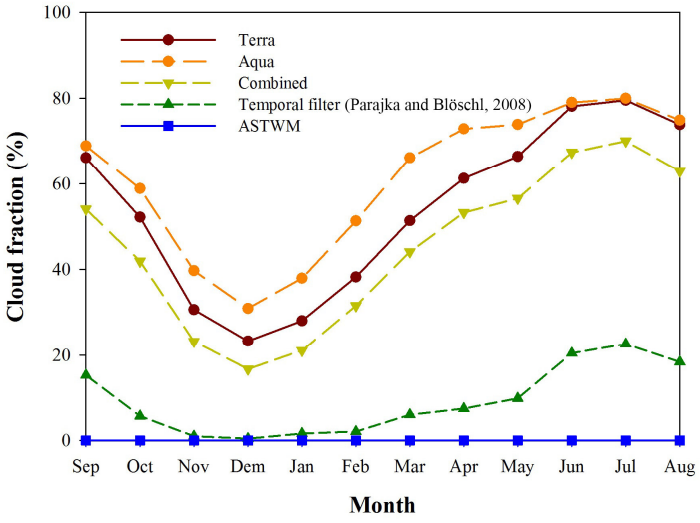

Fig. 3. The average monthly cloud fraction of Terra, Aqua, and the removal results of each step from 2000 to 2014 in the Hengduan Mountains.

4.1.2. Accuracy of the cloud removal methods

Firstly, in the simulated experiments, a comparison was made between ASTWM and the temporal filter with a predefined temporal window of 5 days (Parajka and Blöschl, 2008). In order to ensure the reliability, the clouds of 25 dates of Terra snow cover products (except for

July and August) (see Table 1) were removed. In Table 1, every year several snow cover products with clouds less than 5% are chosen as the observed data during 2001–2013, and then 20%–80% clouds masks from other dates are added to them so that the simulated experiments can be done. Specially, only July and August are not chosen as the validation dates. For an intuitive comparison with the removal results, the two methods were used without the first step (the Terra and Aqua combination). First of all, the visual effects of the cloud removal results of the two methods were compared. For brevity, only two examples are shown in Fig. 4 and Fig. 5, respectively. Fig. 4 shows the results on May 14, 2002, where the simulated cloud fraction was 44.43%. It can be seen that ASTWM removes the clouds completely, while the temporal filter leaves a cloud fraction of 8.27%. Moreover, the temporal filter apparently increases the snow fraction compared to the "truth", especially in the boundary of the western region. In contrast, the ASTWM result is closer to the "truth", except for the fact that the scattered snow pixels in the southern part are not estimated. Fig. 5 shows the results of the two methods on February 22, 2010, with an extraordinarily high cloud fraction of 93.89%. In this case, the temporal filter results in a remaining cloud fraction of 0.25%, which can be ignored. Similarly, the ASTWM result is closer to the "truth", excluding some scattered snow pixels, while the temporal filter overestimates the snow cover, especially in the east. Overall, ASTWM removes the clouds completely, and the results are closer to the "truth" in visual effect than those of the temporal filter.

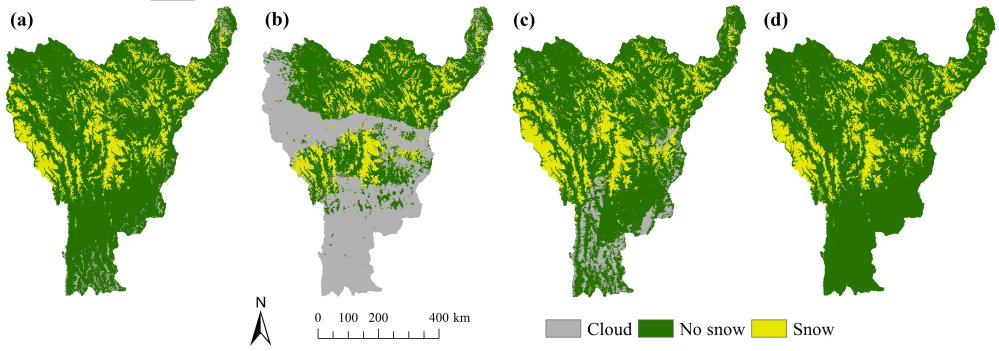

Fig. 4. Cloud removal results on May 14, 2002, in the Hengduan Mountains. (a) The "truth" product. (b) The "observation" product. (c) The result after the temporal filter. (d) The result after ASTWM.

The quantitative evaluation of the two methods is shown in Table 1, with the indicators of OA, OC, UE, and OE. It can be seen that ASTWM performs well on every date, with cloud fractions from 20% to more than 90%. Specifically, ASTWM removes clouds completely, with the average OA/OC reaching 96.08% on average. For all the selected dates, the OA/OC of ASTWM is above 93%, with a highest score of 98.92%, which indicates that ASTWM embodies robustness and universality. It can be seen that the UE is slightly higher than the OE by 2% on average. That is to say, ASTWM has a tendency to assign snow pixels as no snow pixels. Compared with the temporal filter, the OA of ASTWM is 6.68% higher due largely to the temporal filter leaving clouds ranging from 0.01% to 21.02%. In terms of OC, ASTWM is 2.24% higher than the temporal filter on average, except for March 20, 2000, and February 21, 2011. On December 1, 2002, November 11, 2004, and November 17, 2012, the OC of ASTWM is higher than the temporal filter by 2.58%, 1.83%, and 2.44%, respectively, on the condition that the remaining clouds of the temporal filter are negligible. In addition, the UE of the temporal filter is lower than the UE of ASTWM by 0.83% on average, except for November 11, 2004, while the OE of the temporal filter is much higher than the OE of ASTWM by 3.07% on average, except for March 20, 2001, and December 3, 2008. This indicates that when compared with the temporal filter, ASTWM can greatly reduce the OE, while slightly increasing the UE at the same time.

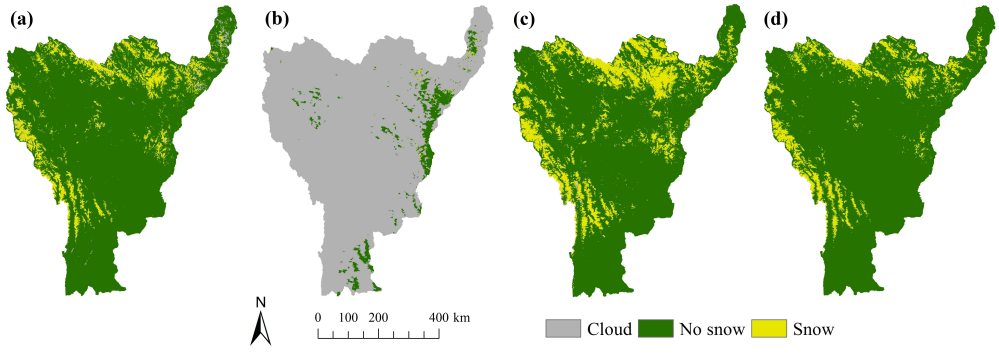

Fig. 5. Cloud removal results on February 22, 2010, in the Hengduan Mountains. (a) The "truth" product. (b) The "observation" product. (c) The result after the temporal filter. (d) The result after ASTWM.

Furthermore, for an in-depth comparison, the proposed ASTWM is compared to the 5-day temporal filter, a combination of 5-day temporal filter and spatial filter (Parajka and Blöschl, 2008), 15-day temporal filter, at the aspects of remaining fraction (RF) of clouds and OA. The three compared methods are called TF(5), TF(5)+SF, and TF(15) in turn in Table 2, which shows the objective evaluations of the cloud removal. On one hand, as far as the RF is concerned, only ASTWM removes clouds completely. For temporal filter, longer temporal window means lower RF, and spatial filter is very helpful to decrease the RF of temporal filter. On the other hand, for OA, ASTWM obtains the highest accuracy among the four methods, and on the whole, a rough ranking from the worst to the best is TF(5), TF(5)+SF, TF(15) and ASTWM. When spatial filter is applied, the OA of 5-day temporal filter is improved for the sake of considering spatial information. Since more temporal reference information is used, 15-day temporal filter has a higher OA than 5-day temporal filter.

Additionally, the cloud removal accuracies of ASTWM with different temporal windows are further analyzed. Table 3 shows the OA of ASTWM with temporal windows by 5 days, 10 days, 15 days, 20 days, 25 days and 30 days. For the same simulated data, the best accuracy is bold. As shown in Table 3, for the shortest temporal window (5 days), it hardly gets the best accuracy. For other temporal windows (10 days, 15 days, 20 days, 25 days, 30 days), they can get the best accuracy more or less. Relatively speaking, the longer temporal window more easily obtains the best OA. Although long time might lose information of short time snow cover, the adaptively temporal weights can relieve this status to some degree. In the experiments, the temporal window is set as 15 days for a tradeoff between accuracy and computational efficiency. Since the accuracy differences with different temporal windows are not obvious, shorter temporal window is recommended for the snow cover information in lower elevations and south facing slopes.

Overall, ASTWM can remove clouds completely, with an excellent OA, and has an advantage over the temporal filter and spatial filter in cloud removal accuracy, despite the fact that it may assign snow pixels as no snow pixels. Since the Terra and Aqua combination obtains the best OC of the present methods, we adopted it before ASTWM in the analysis experiments.

Table 1 The basic details of the selected products and the accuracy of ASTWM in comparison with the 5-day temporal filter in the Hengduan Mountains. CF represents the cloud fraction of the "observations"; RF represents the remaining cloud fraction; TF represents the temporal filter.

Cloud-less dates	Cloud mask dates	CF	RF ↓		OA ↑		OC ↑		UE ↓		OE ↓	
			ASTWM	TF	ASTWM	TF	ASTWM	TF	ASTWM	TF	ASTWM	TF
Mar 20, 2001	Jul 11, 2002	28.86	0.00	5.42	**93.37**	76.46	93.37	**94.03**	5.69	**5.19**	0.95	**0.78**
May 14, 2002	May 14, 2003	44.43	0.00	8.27	**94.67**	74.79	**94.67**	89.99	3.99	**1.32**	1.34	8.69
Dec 1, 2002	Dec 12, 2000	79.70	0.00	0.03	**95.30**	92.70	**95.30**	92.72	3.09	**2.82**	**1.61**	4.46
Jan 13, 2003	Mar 11, 2002	36.35	0.00	0.40	**96.79**	94.46	**96.79**	95.01	1.93	**1.35**	**1.28**	3.64
Apr 19, 2003	May 23, 2004	85.49	0.00	0.85	**96.89**	94.16	**96.89**	95.06	2.30	**1.46**	**0.81**	3.48
Mar 16, 2004	Aug 10, 2002	93.09	0.00	0.93	**95.34**	92.12	**95.34**	92.90	3.24	**3.01**	**1.41**	4.09
May 8, 2004	Dec 4, 2005	21.94	0.00	2.50	**93.49**	81.21	**93.49**	91.93	3.44	**2.22**	**3.07**	5.85
Nov 11, 2004	Oct 22, 2005	93.53	0.00	0.02	**96.02**	94.16	**96.02**	94.17	**3.22**	3.23	**0.76**	2.60
Jan 28, 2005	Feb 14, 2006	61.87	0.00	3.30	**93.17**	89.59	**93.17**	92.54	5.70	**5.14**	**1.13**	2.33
Mar 4, 2007	Oct 7, 2008	55.76	0.00	1.15	**93.11**	90.09	**93.11**	90.90	6.29	**6.07**	**0.60**	3.02
Apr 19, 2007	Jun 6, 2006	72.61	0.00	0.08	**97.79**	94.57	**97.79**	94.67	1.20	**0.42**	**1.01**	4.91
Dec 3, 2008	Sep 21, 2007	43.39	0.00	0.51	**97.00**	94.66	**97.00**	95.19	2.08	**1.46**	**0.92**	3.35
Apr 16, 2009	Apr 12, 2010	34.48	0.00	0.36	**96.17**	95.55	**96.17**	96.08	2.68	**2.53**	**1.45**	1.39
May 20, 2009	Jan 28, 2008	81.01	0.00	12.38	**96.12**	74.10	**96.12**	87.47	3.45	**1.08**	**0.43**	11.45
Oct 29, 2009	Nov 8, 2010	26.61	0.00	1.50	**97.82**	94.18	**97.82**	97.63	1.78	**1.37**	**0.40**	1.00
Feb 22, 2010	Feb 25, 2009	93.89	0.00	0.25	**94.34**	89.83	**94.34**	90.05	3.51	**1.36**	**2.15**	8.58
Mar 17, 2010	Jul 24, 2009	97.81	0.00	4.05	**94.81**	87.44	**94.81**	91.31	4.40	**2.61**	**0.79**	6.08
Dec 21, 2010	Jan 26, 2009	83.67	0.00	0.09	**95.88**	94.65	**95.88**	94.66	**2.91**	3.02	**1.21**	2.31
Mar 1, 2011	Dec 27, 2012	43.00	0.00	0.22	**97.42**	94.97	**97.42**	95.41	1.54	**0.56**	**1.04**	4.03
May 18, 2011	Feb 12, 2012	65.05	0.00	9.15	**98.15**	78.67	**98.15**	91.68	1.20	**0.23**	**0.65**	8.09
Oct 20, 2012	Aug 7, 2013	95.23	0.00	1.09	**98.92**	97.49	**98.92**	98.09	0.74	**0.37**	**0.34**	1.54
Nov 17, 2012	Dec 12, 2013	45.95	0.00	0.01	**97.62**	95.16	**97.62**	95.18	1.86	**1.25**	**0.52**	3.57
Mar 5, 2013	Feb 13, 2014	32.58	0.00	0.28	**95.54**	93.87	**95.54**	94.72	3.80	**3.76**	**0.66**	1.52
May 26, 2013	Apr 25, 2014	84.40	0.00	2.68	**97.17**	93.56	**97.17**	95.72	2.20	**0.98**	**0.63**	3.30
Sep 13, 2013	Oct 3, 2012	89.98	0.00	21.02	**98.83**	74.38	**98.83**	96.18	1.05	**0.33**	**0.12**	3.49
Average		63.63	0.00	3.06	**96.07**	89.31	**96.07**	93.73	2.93	**2.13**	**1.01**	4.14

Note: ↑ means that the higher value represents better result, and ↓ means that the lower value represents better result.

Table 2 The accuracy comparison results of different methods. CF represents the cloud fraction of the "observations"; RF represents the remaining cloud fraction; TF represents the temporal filter, and the number in the bracket represents its temporal window; SF represents the spatial filter (Parajka and Blöschl, 2008)**.**

Cloud-less dates	Cloud mask dates	CF	RF ↓				OA ↑			
			ASTWM	TF(5)	TF(5)+SF	TF(15)	ASTWM	TF(5)	TF(5)+SF	TF(15)
Mar 20, 2001	Jul 11, 2002	28.86	**0.00**	5.42	2.49	**0.00**	**93.37**	76.46	85.61	91.49
May 14, 2002	May 14, 2003	44.43	**0.00**	8.27	4.87	0.28	**94.67**	74.79	82.12	90.22
Dec 1, 2002	Dec 12, 2000	79.70	**0.00**	0.03	0.01	**0.00**	**95.30**	92.70	92.57	92.72
Jan 13, 2003	Mar 11, 2002	36.35	**0.00**	0.40	0.06	0.01	**96.79**	94.46	95.09	94.93
Apr 19, 2003	May 23, 2004	85.49	**0.00**	0.85	0.39	0.08	**96.89**	94.16	94.79	94.87
Mar 16, 2004	Aug 10, 2002	93.09	**0.00**	0.93	0.23	0.02	**95.34**	92.12	92.59	92.70
May 8, 2004	Dec 4, 2005	21.94	**0.00**	2.50	0.90	0.02	**93.49**	81.21	88.12	91.59
Nov 11, 2004	Oct 22, 2005	93.53	**0.00**	0.02	0.00	**0.00**	**96.02**	94.16	93.93	94.17
Jan 28, 2005	Feb 14, 2006	61.87	**0.00**	3.30	1.79	0.05	**93.17**	89.59	90.57	91.92
Mar 4, 2007	Oct 7, 2008	55.76	**0.00**	1.15	0.56	**0.00**	**93.11**	90.09	90.29	90.80
Apr 19, 2007	Jun 6, 2006	72.61	**0.00**	0.08	0.04	**0.00**	**97.79**	94.57	95.36	94.67
Dec 3, 2008	Sep 21, 2007	43.39	**0.00**	0.51	0.15	**0.00**	**97.00**	94.66	95.07	95.13
Apr 16, 2009	Apr 12, 2010	34.48	**0.00**	0.36	0.04	0.06	**96.17**	95.55	96.19	95.95
May 20, 2009	Jan 28, 2008	81.01	**0.00**	12.38	7.21	0.41	**96.12**	74.10	80.64	88.05
Oct 29, 2009	Nov 8, 2010	26.61	**0.00**	1.50	0.70	0.53	**97.82**	94.18	96.17	95.94
Feb 22, 2010	Feb 25, 2009	93.89	**0.00**	0.25	0.04	**0.00**	**94.34**	89.83	90.48	89.96
Mar 17, 2010	Jul 24, 2009	97.81	**0.00**	4.05	2.64	1.86	**94.81**	87.44	88.43	89.34
Dec 21, 2010	Jan 26, 2009	83.67	**0.00**	0.09	0.00	**0.00**	**95.88**	94.65	94.33	94.66
Mar 1, 2011	Dec 27, 2012	43.00	**0.00**	0.22	0.07	**0.00**	**97.42**	94.97	95.53	93.10
May 18, 2011	Feb 12, 2012	65.05	**0.00**	9.15	3.58	0.04	**98.15**	78.67	87.94	92.13
Oct 20, 2012	Aug 7, 2013	95.23	**0.00**	1.09	0.52	0.85	**98.92**	97.49	97.91	97.65
Nov 17, 2012	Dec 12, 2013	45.95	**0.00**	0.01	0.00	**0.00**	**97.62**	95.16	95.18	95.18
Mar 5, 2013	Feb 13, 2014	32.58	**0.00**	0.28	0.13	**0.00**	**95.54**	93.87	94.51	94.70
May 26, 2013	Apr 25, 2014	84.40	**0.00**	2.68	0.64	0.45	**97.17**	93.56	95.36	95.47
Sep 13, 2013	Oct 3, 2012	89.98	**0.00**	21.02	0.64	18.33	**98.83**	74.38	82.71	77.17
Average		63.63	**0.00**	3.06	1.10	0.92	**96.07**	89.31	91.66	92.58

Note: ↑ means that the higher value represents better result, and ↓ means that the lower value represents better result.

Table 3 The overall accuracy (OA ↑) of ASTWM with different temporal windows. CF represents the cloud fraction of the "observations".

Cloud-less dates	Cloud mask dates	CF	5 days	10 days	15 days	20 days	25 days	30 days
Mar 20, 2001	Jul 11, 2002	28.86	87.13	92.45	93.37	93.52	**93.60**	93.51
May 14, 2002	May 14, 2003	44.43	94.71	**94.72**	94.67	94.61	94.63	94.60
Dec 1, 2002	Dec 12, 2000	79.70	95.13	95.29	**95.30**	95.32	95.29	95.23
Jan 13, 2003	Mar 11, 2002	36.35	96.56	96.75	96.79	96.83	**96.85**	96.84
Apr 19, 2003	May 23, 2004	85.49	96.72	96.89	96.89	96.91	96.94	**96.98**
Mar 16, 2004	Aug 10, 2002	93.09	95.22	95.31	95.34	95.38	95.39	**95.40**
May 8, 2004	Dec 4, 2005	21.94	92.50	93.65	93.49	93.84	93.88	**93.95**
Nov 11, 2004	Oct 22, 2005	93.53	95.80	96.00	96.02	96.04	96.05	**96.07**
Jan 28, 2005	Feb 14, 2006	61.87	92.81	93.00	93.17	93.15	**93.20**	93.15
Mar 4, 2007	Oct 7, 2008	55.76	92.53	92.75	93.11	93.11	**93.13**	92.93
Apr 19, 2007	Jun 6, 2006	72.61	97.48	97.49	97.79	98.03	98.05	**98.06**
Dec 3, 2008	Sep 21, 2007	43.39	96.73	96.95	97.00	97.03	**97.04**	**97.04**
Apr 16, 2009	Apr 12, 2010	34.48	96.06	96.14	96.17	**96.18**	96.16	96.16
May 20, 2009	Jan 28, 2008	81.01	95.96	95.91	96.12	96.23	96.33	**96.42**
Oct 29, 2009	Nov 8, 2010	26.61	97.79	**97.84**	97.82	97.76	97.77	97.81
Feb 22, 2010	Feb 25, 2009	93.89	94.14	94.20	94.34	**94.46**	94.45	94.38
Mar 17, 2010	Jul 24, 2009	97.81	94.69	94.78	94.81	94.77	94.81	**94.85**
Dec 21, 2010	Jan 26, 2009	83.67	95.62	95.82	95.88	**95.91**	**95.91**	**95.91**
Mar 1, 2011	Dec 27, 2012	43.00	97.32	**97.44**	97.42	97.37	97.36	97.35
May 18, 2011	Feb 12, 2012	65.05	97.80	**98.15**	**98.15**	**98.15**	98.14	98.12
Oct 20, 2012	Aug 7, 2013	95.23	98.84	98.89	98.92	98.93	98.94	**98.95**
Nov 17, 2012	Dec 12, 2013	45.95	97.51	97.55	97.62	97.66	**97.68**	**97.68**
Mar 5, 2013	Feb 13, 2014	32.58	95.25	95.47	95.54	95.60	95.64	**95.66**
May 26, 2013	Apr 25, 2014	84.40	96.67	97.01	**97.17**	97.14	97.11	97.13
Sep 13, 2013	Oct 3, 2012	89.98	98.74	98.79	98.83	98.83	98.82	**98.85**
Average		63.63	95.59	95.97	96.07	96.11	**96.13**	96.12

4.2. Variability of snow cover

4.2.1. Snow cover days (SCD)

SCD reflects the spatial distribution of the snow cover in a hydrologic year. Fig. 6(a) shows the average SCD from 2000 to 2014 in the Hengduan Mountains, which is positively correlated with elevation (R=0.47). The SCD of less than 60 days occupies the most area, at about 84.32%, and is regarded as the unstable snow cover area. In contrast, the SCD of over 60 days, at only 15.68%, is regarded as the stable snow cover area and the source of the water resource. The SCD of over 240 days, occupying 0.34%, is mainly in the peaks of the high mountains (above 4500m), including Gaoligong, Yunling, Qionglai, and Daxue mountains. In the surroundings of the area with SCD of over 240 days, the SCD gradually decreases as the elevation decreases, forming belts along the mountain ranges. The CV based on the multi-annual SCD is shown in Fig. 6(b). The greater the CV, the stronger the inter-annual fluctuation. The inter-annual fluctuation greatly decreases as the elevation increases, and the CV exhibits a negative linear correlation with elevation (R=−0.56). In conclusion, the SCD increases and the CV decreases as the elevation increases in most parts of the study area, indicating that the snow cover is relatively stable in the high elevation areas and the inter-annual fluctuation is greatest in the low elevation areas.

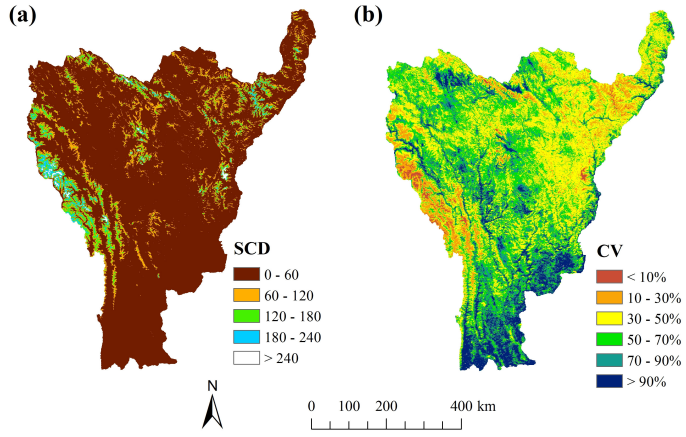

Fig. 6. The SCD and the CV from 2000 to 2014 in the Hengduan Mountains. (a) The spatial distribution of the mean SCD. (b) The spatial distribution of the CV.

We also analyzed the pixel-wise trends of SCD using the piecewise linear regression model. The breakpoints of the trends mainly occur between 2004/2005 and 2008/2009 [Fig. 7(a)]. Overall, the SCD shows an increasing trend in 93.74% of the study region before the breakpoint, with an average increase of +5.20 days yr^{-1} [Fig. 7(b)]. In contrast, the SCD shows a decreasing trend after the breakpoint in 83.60% of the area, with an average rate of change of −3.00 days yr^{-1} [Fig. 7(c)]. It is worth mentioning that the distributions of the trends before and after the breakpoints are similar. In summary, the pixel-wise trends of the SCD before the breakpoints are mainly positive, while the trends after the breakpoints are mainly negative.

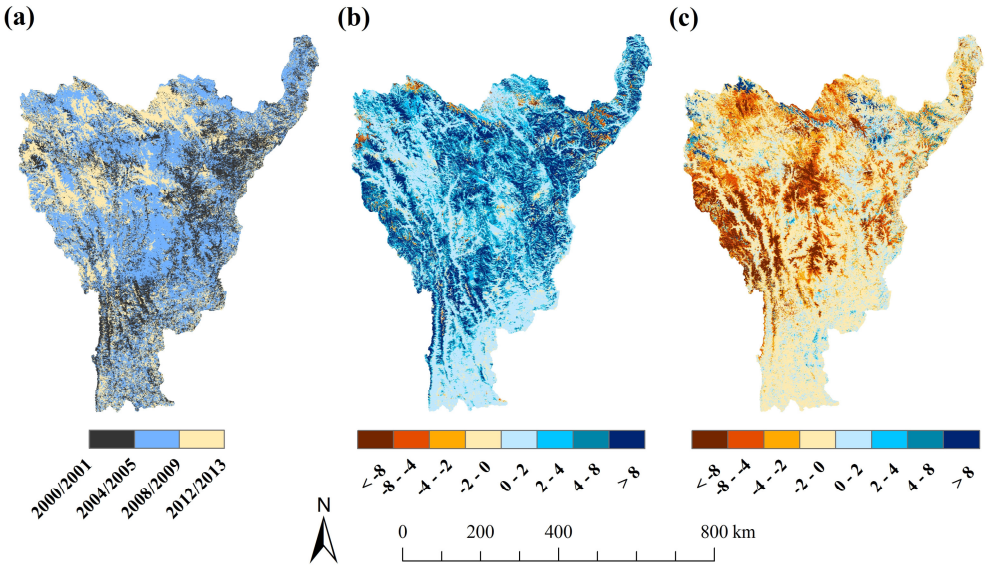

Fig. 7. The pixel-wise trends of the SCD. (a) The breakpoints of the trends. (b) The trends before the breakpoints. (c) The trends after the breakpoints in the Hengduan Mountains.

4.2.2. Snow fraction

The snow fraction is widely used to analyze the intra-annual and inter-annual variability of snow cover. Fig. 8 shows the intra-annual variability of snow cover in the Hengduan Mountains, according to the average daily snow fraction from 2000 to 2014, in which the error bars represent the standard deviation. The snow cover is mainly concentrated from late October to late March. During this period, the snow fraction is always greater than 10%, with large

standard deviations, which indicates that the variability is high. In late November, the snow fraction peaks at a maximum of 24.33%. From early December to late February, the snow fraction fluctuates slightly, and remains around 13% due to the low precipitation. In early March, there is another peak of 19.97%. From late March, the snow gradually melts. In general, the peak of the snow fraction reaches only 25% (in November), and the intra-annual variability is significant over the hydrologic year, especially from late October to late March.

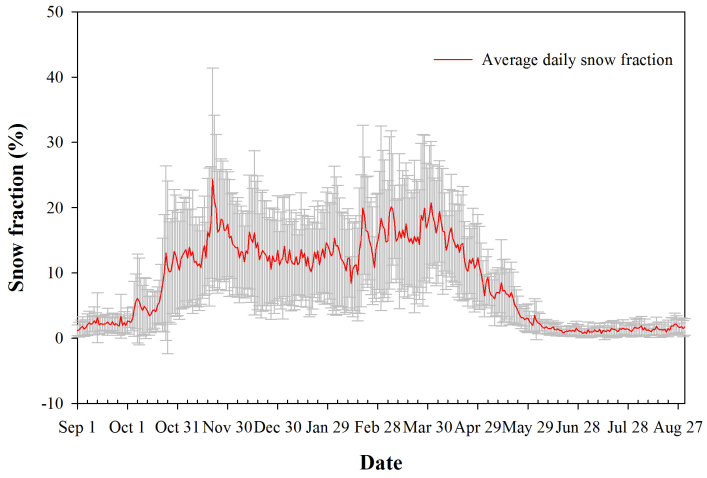

Fig. 8. The intra-annual variability of the snow fraction from 2000 to 2014 in the Hengduan Mountains.

The inter-annual variability of the average annual snow fraction from 2000 to 2014 is shown in Fig. 9. The inter-annual variability fluctuates greatly. Using the piecewise linear regression model, it is apparent that there is an increasing trend of +1.14% yr^{-1} from 2000/2001 to 2004/2005 and a decreasing trend of –0.25% yr^{-1} from 2004/2005 to 2013/2014. During the increasing period, the minimum average annual snow fraction is 6.12% in 2001/2002 and the maximum is 11.27% in 2004/2005. Additionally, during the decreasing period, the maximum average annual snow fraction is 11.27% in 2004/2005 and the minimum is 6.63% in 2012/2013. The decreasing trend is clearly slower than the increasing trend.

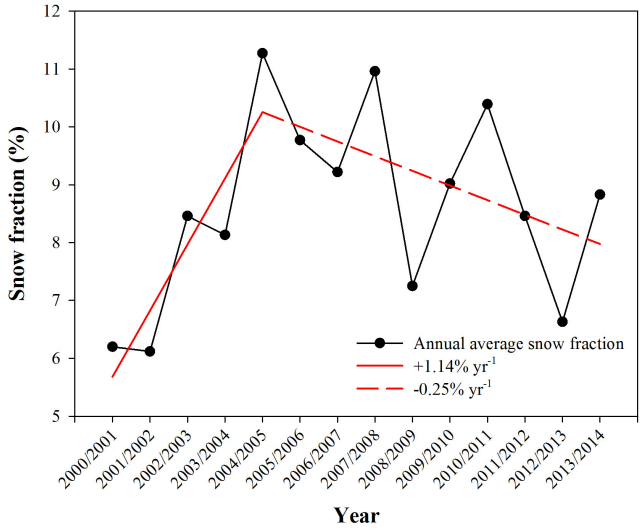

Fig. 9. The inter-annual variability of the snow fraction from 2000 to 2014 in the Hengduan Mountains.

4.3. The response of snow cover to climate change

Climate change is one of the major drivers for snow cover variability (Immerzeel et al., 2009; Gao et al., 2012). It is therefore necessary to analyze the relationship between air temperature, precipitation, and snow cover, as well as explain how snow cover responds to climate change. On the one hand, from the average monthly snow fraction and air temperature from 2000 to 2014 [Fig. 10(a)], it is clear that when the air temperature decreases, the snow fraction increases, and vice versa. On the other hand, from the average monthly snow fraction and precipitation from 2000 to 2014 [Fig. 10(b)], the variation of the snow fraction and precipitation is very similar to the variation of the air temperature. These phenomena reveal that the inter-annual variation of snow cover shows a negative correlation to air temperature and precipitation.

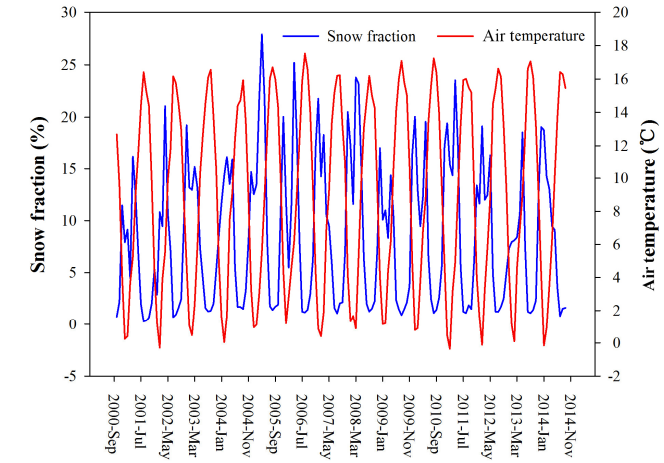

(a)

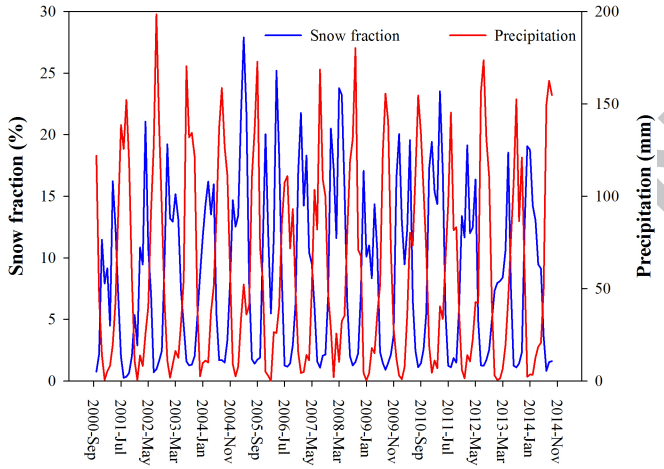

(b)

Fig. 10. The intra-annual variation of the snow fraction and two climate factors from 2000 to 2014 in the Hengduan Mountains. (a) The average monthly snow fraction and air temperature. (b) The average monthly snow fraction and precipitation.

The inter-annual Pearson correlation coefficients (PCCs) for the average monthly snow fraction and air temperature/precipitation from October to March are shown in Table 4. In October, temperature clearly has a better correlation than precipitation with the snow fraction. From November to December, the PCCs of precipitation are larger than those of air temperature. As a result, precipitation is the primary factor affecting the snow cover variation. From January to February, the temperature gradually increases, but is still low when the precipitation becomes sufficient to accelerate the formation and sublimation of snow cover. In

March, the PCCs of both air temperature and precipitation are very high and similar, embodying the fact that they have a balanced influence on snow cover variation. Interestingly, the average snow fraction from October to March has a weak negative correlation with air temperature and a strong positive correlation with precipitation. It is therefore suggested that when compared with temperature, precipitation plays a dominant role in the variability of snow cover as a whole.

Table 4 The Pearson correlation coefficients for the average monthly snow fraction and air temperature/precipitation (October to March) from 2000 to 2014 in the Hengduan Mountains.

Months	Air temperature	Precipitation
October	−0.43	+0.29
November	−0.10	+0.33
December	−0.36	+0.41
January	−0.55*	+0.37
February	−0.79**	+0.38
March	−0.63	+0.66**
Average	−0.12	+0.66**

** and * represent the statistical significance at the 0.01 and 0.05 levels, respectively.

5. Discussion and conclusion

This work has proposed an adaptive spatio-temporal weighted method (ASTWM) to remove clouds completely from MODIS snow cover products. To ensure a better accuracy, a Terra and Aqua combination is introduced as the first step prior to ASTWM. The Terra/Aqua combination step can reduce the cloud cover by 7% to 13%, and its high accuracy in clear-sky conditions has been validated by many researchers (Parajka and Blöschl, 2008; Wang et al., 2009; Gao et al., 2010; López-Burgos et al., 2013). ASTWM is based on snow cover probability, and it makes the best use of the spatial and temporal correlations of snow cover. Compared with the currently successive utilization of the two types of correlations, ASTWM undertakes a joint utilization. For the cloud removal of snow cover products, it can be used as

a separate method and also in combination with other methods. As shown in the simulated experiments with different cloud conditions, ASTWM performs well, obtaining an average OA of 96.07%, which is better than the temporal filter and spatial filter. In conclusion, ASTWM has the following advantages when used in mountainous regions: 1) it can remove clouds completely; 2) it simultaneously considers the spatial topography and the temporal sustainability of snow cover; and 3) owing to the absence of snow cover subcycles in a hydrologic year, it has a superiority in the snow melt and accumulation period. However, ASTWM also has some disadvantages. For example, in some circumstances, it may assign snow pixels as no snow pixels by mistake. This is likely a result of darker conditions caused by the shading of terrain and vegetation cover (Krajčí et al., 2014). In addition, its time cost is a little high when compared to the present methods, due to the computational complexity of the weight solution. A better tradeoff mechanism of accuracy and efficiency is needed in the near future.

Based on the two steps, a cloud-free MODIS snow cover product was generated to investigate the spatio-temporal variability of snow cover in the Hengduan Mountains from 2000 to 2014. In this work, the variability was monitored from the aspects of snow cover days (SCD) and snow fraction. It was found that SCD was positively correlated with elevation and CV was negatively correlated with elevation. This indicates that the higher the elevation, the less the inter-annual variability of SCD. This phenomenon is in accordance with the innovative work by Krajčí et al (2016) in Slovak basins, in which they find that snow cover area and duration increases with increasing mean basin elevation by three groups of basins. Furthermore, based on the piecewise linear regression model, the pixel-wise trends of SCD were established. The trends before the breakpoints are 93.74% positive and the trends after the breakpoints are 83.60% negative, especially in the high elevation area. This is clearly similar to the inter-annual variability of the snow fraction. As far as the snow fraction is concerned, the intra-annual variability is particularly intense from late October to late March. The peaks of the snow fraction usually happen in November and March, reaching around 25% and 20%,

respectively. Furthermore, the inter-annual variability was divided into two periods by a piecewise linear regression model, showing an increasing trend of +1.14% yr^{-1} before 2004/2005 and a decreasing trend of –0.25% yr^{-1} after 2004/2005. The snow fraction also increases with elevation, and the variation trend becomes more significant.

It is well known that snow cover is very sensitive to climate change, e.g., atmospheric circulation, air temperature, precipitation, wind, and solar radiation. In comparison, air temperature and precipitation are the most important factors for the variability of snow cover, which can identify the temporal climatic controls and enable long-term versus short-term trend detection (Crawford et al., 2013). Thus, the intra-annual and inter-annual variability of snow cover can be explained by the relationship between air temperature, precipitation, and snow fraction. For the intra-annual variability, the snow fraction increases when the air temperature and precipitation decrease, and the relationships are stable. For the inter-annual variability, according to the Pearson correlation coefficients, in October, air temperature affects the formation and accumulation of snow cover more strongly than precipitation. In contrast, in November and December, precipitation is the primary factor accounting for the variability of snow cover. From January to February, the air temperature is the dominant factor accelerating the formation and sublimation of snow cover. In March, air temperature and precipitation both influence snow cover. On the whole, from October to March, precipitation plays a leading role in the variation of snow cover when compared to air temperature. However, due to the huge changes of both elevation and latitude, Hengduan Mountains feature a very variable climate, in which the local variation may be inconsistent with the overall variation. In conclusion, under the background of global warming, the air temperature in the Hengduan Mountains has shown little change from 2000 to 2014. Meanwhile, there has been a large reduction in inter-annual precipitation from 2005, which predominantly accounts for the decreased snow cover. If the snow cover continues to decline, the water resource will decrease, the biology of the area will change, and the ecology will be adversely affected. For the future work, more detailed analysis will be conducted with the help of the *in situ* observations of snow depth, it's because

the advantages in the analysis on the temporal variations.

Additionally, Version 6 MODIS snow cover data sets are now available at the NASA NSIDC Distributed Active Archive Center (DAAC). In this version, Fractional Snow Cover has been replaced by Normalized Difference Snow Index (NDSI) snow cover. For the new MODIS 006 products, the proposed ASTWM method should be modified accordingly. The weights should be applied to the NDSI, rather than the spatial or temporal probability. The key point is to compute the spatial weights and temporal weights.

Acknowledgements

The work was supported by the Open Research Fund of Key Laboratory of Digital Earth Science, Institute of Remote Sensing and Digital Earth, Chinese Academy of Sciences under Grant No. 2016LDE004, the National Natural Science Foundation of China (NSFC) under Grant No. 41422108, the Fundamental Research Funds for the Central Universities under Grant No. 2042017kf0034, and the Key Laboratory of Satellite Mapping Technology and Application, National Administration of Surveying, Mapping and Geoinformation under Grant No. KLSMTA-201703. The authors would also like to thank the anonymous reviewers.

References

Barnett, T., Dümenil, L., Schlese, U., Roeckner, E. and Latif, M., 1989. The effect of Eurasian snow cover on regional and global climate variations. Journal of the Atmospheric Sciences, 46(5): 661-686.

Barnett, T., Dumenil, L., Schlese, U. and Roeckner, E., 1988. The effect of Eurasian snow cover on global climate. Science, 239(4839): 504-507.

Barnett, T.P., Adam, J.C. and Lettenmaier, D.P., 2005. Potential impacts of a warming climate on water availability in snow-dominated regions. Nature, 438(7066): 303-309.

Bitner, D., Carroll, T., Cline, D. and Romanov, P., 2002. An assessment of the differences between three satellite snow cover mapping techniques. Hydrological Processes, 16(18): 3723-3733.

Brown, R.D., 2000. Northern Hemisphere snow cover variability and change, 1915-97. Journal of Climate, 13(13): 2339-2355.

Cheng, Q., Liu, H., Shen, H., Wu, P. and Zhang, L., Spatial and Temporal Nonlocal Filter-Based Data Fusion Method. IEEE Transactions on Geoscience and Remote Sensing: DOI: 10.1109/TGRS.2017.2692802.

Cheng, Q., Shen, H., Zhang, L. and Li, P., 2014. Inpainting for Remotely Sensed Images With a Multichannel Nonlocal Total Variation Model. IEEE Transactions on Geoscience and Remote Sensing, 52(1): 175-187.

Crawford, C.J., Manson, S.M., Bauer, M.E. and Hall, D.K., 2013. Multitemporal snow cover mapping in mountainous terrain for Landsat climate data record development. Remote Sensing of Environment,

135: 224-233.
Déry, S.J., Salomonson, V.V., Stieglitz, M., Hall, D.K. and Appel, I., 2005. An approach to using snow areal depletion curves inferred from MODIS and its application to land surface modelling in Alaska. Hydrological Processes, 19(14): 2755-2774.
Da Ronco, P. and De Michele, C., 2014. Cloud obstruction and snow cover in Alpine areas from MODIS products. Hydrology and Earth System Sciences, 18(11): 4579-4600.
Dahe, Q., Shiyin, L. and Peiji, L., 2006. Snow cover distribution, variability, and response to climate change in western China. Journal of Climate, 19(9): 1820-1833.
Dietz, A.J., Wohner, C. and Kuenzer, C., 2012. European snow cover characteristics between 2000 and 2011 derived from improved MODIS daily snow cover products. Remote Sensing, 4(8): 2432-2454.
Flerchinger, G., Cooley, K. and Ralston, D., 1992. Groundwater response to snowmelt in a mountainous watershed. Journal of Hydrology, 133(3-4): 293-311.
Gafurov, A. and Bárdossy, A., 2009. Cloud removal methodology from MODIS snow cover product. Hydrology and Earth System Sciences, 13(7): 1361-1373.
Gao, J., Williams, M.W., Fu, X., Wang, G. and Gong, T., 2012. Spatiotemporal distribution of snow in eastern Tibet and the response to climate change. Remote Sensing of Environment, 121: 1-9.
Gao, Y., Xie, H., Yao, T. and Xue, C., 2010. Integrated assessment on multi-temporal and multi-sensor combinations for reducing cloud obscuration of MODIS snow cover products of the Pacific Northwest USA. Remote Sensing of Environment, 114(8): 1662-1675.
Gascoin, S., Hagolle, O., Huc, M., Jarlan, L., Dejoux, J.-F., Szczypta, C., Marti, R. and Sánchez, R., 2015. A snow cover climatology for the Pyrenees from MODIS snow products. Hydrology and Earth System Sciences, 19: 2337-2351.
Hall, D., Riggs, G. and Salomonson, V., 2007. MODIS/Terra Aqua Snow Cover Daily L3 Global 500 m Grid V005. Digital Media, National Snow and Ice Data Center, Boulder, Colorado, USA.
Hall, D.K., Riggs, G.A., Foster, J.L. and Kumar, S.V., 2010. Development and evaluation of a cloud-gap-filled MODIS daily snow-cover product. Remote Sensing of Environment, 114(3): 496-503.
Hall, D.K., Riggs, G.A., Salomonson, V.V., Barton, J., Casey, K., Chien, J., DiGirolamo, N., Klein, A., Powell, H. and Tait, A., 2001. Algorithm theoretical basis document (ATBD) for the MODIS snow and sea ice-mapping algorithms. NASA GSFC.
Hall, D.K., Riggs, G.A., Salomonson, V.V., DiGirolamo, N.E. and Bayr, K.J., 2002. MODIS snow-cover products. Remote Sensing of Environment, 83(1): 181-194.
Immerzeel, W.W., Droogers, P., De Jong, S. and Bierkens, M., 2009. Large-scale monitoring of snow cover and runoff simulation in Himalayan river basins using remote sensing. Remote Sensing of Environment, 113(1): 40-49.
Jin, X., Ke, C.-Q., Xu, Y.-Y. and Li, X.-C., 2015. Spatial and temporal variations of snow cover in the Loess Plateau, China. International Journal of Climatology, 35(8): 1721-1731.
Klein, A.G. and Barnett, A.C., 2003. Validation of daily MODIS snow cover maps of the Upper Rio Grande River Basin for the 2000-2001 snow year. Remote Sensing of Environment, 86(2): 162-176.
Krajčí, P., Holko, L. and Parajka, J., 2016. Variability of snow line elevation, snow cover area and depletion in the main Slovak basins in winters 2001–2014. Journal of Hydrology and Hydromechanics, 64(1): 12-22.
Krajčí, P., Holko, L., Perdigão, R.A.P. and Parajka, J., 2014. Estimation of regional snowline elevation (RSLE) from MODIS images for seasonally snow covered mountain basins. Journal of Hydrology, 519, Part B: 1769-1778.
López-Burgos, V., Gupta, H. and Clark, M., 2013. Reducing cloud obscuration of MODIS snow cover area products by combining spatio-temporal techniques with a probability of snow approach. Hydrology and Earth System Sciences, 17(5): 1809-1823.
Li, X., Shen, H., Li, H. and Zhang, L., 2016. Patch Matching-Based Multitemporal Group Sparse Representation for the Missing Information Reconstruction of Remote-Sensing Images. IEEE Journal of Selected Topics in Applied Earth Observations and Remote Sensing, 9(8): 3629-3641.
Li, X., Shen, H., Zhang, L. and Li, H., 2015. Sparse-based reconstruction of missing information in remote sensing images from spectral/temporal complementary information. ISPRS Journal of Photogrammetry and Remote Sensing, 106: 1-15.
Li, X., Shen, H., Zhang, L., Zhang, H., Yuan, Q. and Yang, G., 2014. Recovering Quantitative Remote Sensing Products Contaminated by Thick Clouds and Shadows Using Multitemporal Dictionary Learning. IEEE Transactions on Geoscience and Remote Sensing, 52(11): 7086-7098.
Liang, T.G., Huang, X.D., Wu, C.X., Liu, X.Y., Li, W.L., Guo, Z.G. and Ren, J.Z., 2008. An application of MODIS data to snow cover monitoring in a pastoral area: A case study in Northern Xinjiang, China.

Remote Sensing of Environment, 112(4): 1514-1526.
Marchane, A., Jarlan, L., Hanich, L., Boudhar, A., Gascoin, S., Tavernier, A., Filali, N., Le Page, M., Hagolle, O. and Berjamy, B., 2015. Assessment of daily MODIS snow cover products to monitor snow cover dynamics over the Moroccan Atlas mountain range. Remote Sensing of Environment, 160: 72-86.
Maskey, S., Uhlenbrook, S. and Ojha, S., 2011. An analysis of snow cover changes in the Himalayan region using MODIS snow products and in-situ temperature data. Climatic Change, 108(1-2): 391-400.
Parajka, J. and Blöschl, G., 2006. Validation of MODIS snow cover images over Austria. Hydrology and Earth System Sciences Discussions, 3(4): 1569-1601.
Parajka, J. and Blöschl, G., 2008. Spatio-temporal combination of MODIS images–potential for snow cover mapping. Water Resources Research, 44(3): W03406(1-13).
Parajka, J. and Blöschl, G., 2012. MODIS-based snow cover products, validation, and hydrologic applications, Multiscale Hydrologic Remote Sensing: Perspectives and Applications. CRC Press, pp. 185-212.
Parajka, J., Holko, L., Kostka, Z. and Blöschl, G., 2012. MODIS snow cover mapping accuracy in a small mountain catchment-comparison between open and forest sites. Hydrology and Earth System Sciences, 16(7): 2365-2377.
Parajka, J., Pepe, M., Rampini, A., Rossi, S. and Blöschl, G., 2010. A regional snow-line method for estimating snow cover from MODIS during cloud cover. Journal of Hydrology, 381(3): 203-212.
Paudel, K.P. and Andersen, P., 2011. Monitoring snow cover variability in an agropastoral area in the Trans Himalayan region of Nepal using MODIS data with improved cloud removal methodology. Remote Sensing of Environment, 115(5): 1234-1246.
Pauli, J.N., Zuckerberg, B., Whiteman, J.P. and Porter, W., 2013. The subnivium: a deteriorating seasonal refugium. Frontiers in Ecology and the Environment, 11(5): 260-267.
Riggs, G.A., Hall, D.K. and Salomonson, V.V., 2006. MODIS snow products user guide to collection 5. Digital Media, 80(6): 1-80.
Robinson, D.A., Dewey, K.F. and Heim Jr, R.R., 1993. Global snow cover monitoring: An update. Bulletin of the American Meteorological Society, 74(9): 1689-1696.
Salomonson, V.V. and Appel, I., 2006. Development of the Aqua MODIS NDSI fractional snow cover algorithm and validation results. IEEE Transactions on Geoscience and Remote Sensing, 44(7): 1747-1756.
Sharma, V., Mishra, V. and Joshi, P., 2014. Topographic controls on spatio-temporal snow cover distribution in Northwest Himalaya. International Journal of Remote Sensing, 35(9): 3036-3056.
Shen, H., Li, X., Cheng, Q., Zeng, C., Yang, G., Li, H. and Zhang, L., 2015. Missing information reconstruction of remote sensing data: A technical review. IEEE Geoscience and Remote Sensing Magazine, 3(3): 61-85.
Simic, A., Fernandes, R., Brown, R., Romanov, P. and Park, W., 2004. Validation of VEGETATION, MODIS, and GOES+ SSM/I snow-cover products over Canada based on surface snow depth observations. Hydrological Processes, 18(6): 1089-1104.
Singh, P., Arora, M. and Goel, N., 2006. Effect of climate change on runoff of a glacierized Himalayan basin. Hydrological Processes, 20(9): 1979-1992.
Şorman, A., Akyürek, Z., Şensoy, A., Şorman, A. and Tekeli, A., 2007. Commentary on comparison of MODIS snow cover and albedo products with ground observations over the mountainous terrain of Turkey. Hydrology and Earth System Sciences, 11(4): 1353-1360.
Tang, Z., Wang, J., Li, H. and Yan, L., 2013. Spatiotemporal changes of snow cover over the Tibetan plateau based on cloud-removed moderate resolution imaging spectroradiometer fractional snow cover product from 2001 to 2011. Journal of Applied Remote Sensing, 7(1): 073582(1-14).
Toms, J.D. and Lesperance, M.L., 2003. Piecewise regression: a tool for identifying ecological thresholds. Ecology, 84(8): 2034-2041.
Tong, J., Déry, S. and Jackson, P., 2009a. Interrelationships between MODIS/Terra remotely sensed snow cover and the hydrometeorology of the Quesnel River Basin, British Columbia, Canada. Hydrology and Earth System Sciences, 13(8): 1439-1452.
Tong, J., Déry, S. and Jackson, P., 2009b. Topographic control of snow distribution in an alpine watershed of western Canada inferred from spatially-filtered MODIS snow products. Hydrology and Earth System Sciences, 13(3): 319-326.
Wang, W., Huang, X., Deng, J., Xie, H. and Liang, T., 2015. Spatio-Temporal Change of Snow Cover and Its Response to Climate over the Tibetan Plateau Based on an Improved Daily Cloud-Free Snow Cover Product. Remote Sensing, 7(1): 169-194.

Wang, X., Piao, S., Ciais, P., Li, J., Friedlingstein, P., Koven, C. and Chen, A., 2011. Spring temperature change and its implication in the change of vegetation growth in North America from 1982 to 2006. Proceedings of the National Academy of Sciences, 108(4): 1240-1245.

Wang, X. and Xie, H., 2009. New methods for studying the spatiotemporal variation of snow cover based on combination products of MODIS Terra and Aqua. Journal of Hydrology, 371(1): 192-200.

Wang, X., Xie, H., Liang, T. and Huang, X., 2009. Comparison and validation of MODIS standard and new combination of Terra and Aqua snow cover products in northern Xinjiang, China. Hydrological Processes, 23(3): 419-429.

Xie, H., Wang, X. and Liang, T., 2009. Development and assessment of combined Terra and Aqua snow cover products in Colorado Plateau, USA and northern Xinjiang, China. Journal of Applied Remote Sensing, 3(1): 033559(1-14).

Zeng, C., Shen, H. and Zhang, L., 2013. Recovering missing pixels for Landsat ETM+ SLC-off imagery using multi-temporal regression analysis and a regularization method. Remote Sensing of Environment, 131: 182-194.

Highlights

- Proposing an adaptively spatio-temporal weighted method for cloud removal.
- Cloud removed completely with an average overall accuracy of 96.07%.
- Intense intra-annual and inter-annual variability of snow cover in Hengduan Mountains.
- Snow cover change responding well to air temperature and precipitation.